Chemical Engineering Journal 157 (2010) 86–92

Contents lists available at ScienceDirect

Chemical Engineering Journal

journal homepage: www.elsevier.com/locate/cej

Characterization, activity and kinetics of a visible light driven photocatalyst: Cerium and nitrogen co-doped TiO_2 nanoparticles

Tao Yu [a,*], Xin Tan [a,b,*], Lin Zhao [a], Yuxin Yin [b], Peng Chen [a], Jing Wei [a]

[a] School of Environmental Science and Engineering, Tianjin University, No. 92, Weijin Road, Nankai District, Tianjin 300072, China
[b] School of Chemical Engineering, Tianjin University, Tianjin 300072, China

ARTICLE INFO

Article history:
Received 2 July 2009
Received in revised form 19 October 2009
Accepted 26 October 2009

Keywords:
TiO_2
Cerium doping
Nitrogen doping
Photocatalyst
Visible light

ABSTRACT

In order to effectively photocatalytically degrade azo dye under solar irradiation, anatase TiO_2 that was co-doped with cerium and nitrogen ($Ti_{1-x}Ce_xO_{1-y}N_y$) nanoparticles (NPs) were synthesized using a one-step technique with a modified sol–gel process. The crystal structure and chemical properties were characterized using XRD, BET and XPS. Oxynitride species, Ce^{4+}/Ce^{3+} pairs, and Ti–O–N and Ti–O–Ce bonds were determined using XPS. The photocatalytic mechanism was investigated through methylene blue (MB) photocatalytic degradation using various filtered wavelengths of light ($\lambda > 365$ nm, $\lambda > 420$ nm, $\lambda > 500$ nm, $\lambda > 550$ nm and $\lambda > 600$ nm) for a period of 10 h. Two experimental parameters were studied systematically, namely the atomic ratio of doped N to Ce and the irradiation wavelength number. The photocatalytic degradation of MB over $Ti_{1-x}Ce_xO_{1-y}N_y$ NPs in aqueous suspension was found to follow approximately first-order kinetics according to the Langmuir–Hinshelwood model. The enhanced photocatalytic degradation was attributed to the increased number of photogenerated •OH radicals.

1. Introduction

Titanium dioxide has been applied as a promising environmentally friendly photocatalyst in many fields such as environmental remediation, hydrogen production and solar energy utilization [1–7]. Titanium dioxide is valued for its chemical stability, lack of toxicity and low cost. Recently, there has been increasing interest in the application of TiO_2 nanoparticles (NPs) in the field of organic and inorganic pollutant removal from wastewater. These practical applications, however, have been limited by the large energy band gap (3.2 eV), which can capture only less than 3% of the available solar energy ($\lambda < 387$ nm), as well as by the fast recombination of photogenerated electron–hole (e^-–h^+) pairs, both on the surface and in the core of TiO_2 NPs. Photocatalysts that function in the visible wavelengths ($400\text{ nm} < \lambda < 800\text{ nm}$) are desirable from the viewpoint of solar energy utilization.

Many attempts have been made to enhance the utilization of solar energy and to inhibit the recombination of photogenerated e^-–h^+ pairs by doping the base photocatalyst with impurities. In the past, transition metal ions and noble metal ions have been used as dopants to broaden optical absorption in the visible light band for practical applications [8,9]. Lanthanide (Ln)-doped TiO_2 NPs have been especially favored for their unique 4f electron configuration. Among others, Ce-doped TiO_2 NPs have attracted interest due to their Ce^{3+}/Ce^{4+} redox couple, which results from the shift of cerium oxide between CeO_2 and Ce_2O_3 under oxidizing and reducing conditions [10–13]. Lanthanide-doped photocatalysts, however, suffer from utilization within the visible light spectrum [14,15]. Sato et al. reported that NO_x species can induce the band gap of TiO_2 to narrow greatly, which broadens its absorption spectra within the visible light region. This research sparked a growing interest in non-metal doping of TiO_2 NPs [16–18]. Among the possibilities, N-doped TiO_2 exhibits significant photocatalytic activities in various reactions under visible light [19–24]. Lattice oxygen atoms can be replaced by doping non-metal elements and hence induce visible light absorption by the modified TiO_2 NPs. Nitrogen-doped TiO_2 NPs, however, are limited by long-term instability, low reactivity and low quantum efficiency [25]. In order to solve these problems, many valuable efforts have been devoted to investigate the synthesis of TiO_2 NPs co-doped with N and Ln elements. For example, it was reported that nitrogen and lanthanum (La) co-doped TiO_2 NPs show superior photocatalytic activity on the photocatalytic degradation of methyl orange under visible light irradiation when compared to only N-doped TiO_2 or Ln-doped TiO_2 [26–28].

In the work presented here, $Ti_{1-x}Ce_xO_{1-y}N_y$ NPs were synthesized, and an aqueous solution of azo dye and methylene blue (MB) was selected as a model pollutant to test photocatalytic activity under various filtered wavelengths of light ($\lambda > 365$ nm, $\lambda > 420$ nm, $\lambda > 500$ nm, $\lambda > 550$ nm and $\lambda > 600$ nm). Two experimental parameters were studied, namely the atomic ratio of doped N to Ce and the irradiation wavelength number. The possible mechanisms and synergistic effects of co-doping N and Ce were discussed in detail.

* Corresponding author. Tel.: +86 22 27891291; fax: +86 22 27401819.
E-mail address: lisat.yu@gmail.com (T. Yu).

1385-8947/$ – see front matter © 2009 Elsevier B.V. All rights reserved.
doi:10.1016/j.cej.2009.10.051

2. Experimental

2.1. Materials

Titanium tetrabutoxide (Sigma–Aldrich, >97%) and cerium nitrate hexahydrate (Sigma–Aldrich, >99%) were used as the starting materials. Urea (Sigma–Aldrich, >99%) was used as the source of nitrogen. All reagents were used as received without any further purification.

2.2. Photocatalyst preparation

Bare TiO_2 (denoted as BT) NPs and cerium and nitrogen co-doped TiO_2 (denoted as $Ti_{1-x}Ce_xO_{1-y}N_y$) NPs were synthesized using a one-step modified sol–gel technique. First, 8.5 ml titanium tetrabutoxide was dissolved in 40 ml absolute ethanol and stirred for 30 min to get a homogeneous solution. Cerium nitrate hexahydrate (0.021 g) and various amount of urea (1.0 g, 2.0 g and 3.0 g, respectively) were dissolved in a mixture of absolute ethanol (20 ml) and double distilled water (2 ml). Then the mixture of cerium nitrate hexahydrate with various amounts of urea was dropped (30 drop/min) into the titanium tetrabutoxide solution while stirring rapidly at room temperature. The resulting solution was stirred continuously until a transparent gel formed. Then the gel was put into a 70 °C oven for 2 days to evaporate the ethanol, which was followed by calcination at 550 °C for 2 h in open air to obtain the desired NPs. The values of x and y were determined by XPS.

2.3. Characterization

X-ray diffraction analysis (XRD) with a CuKa (λ = 1.5406 Å) radiation source over the scan range of 2θ between 10° and 90°, an accelerating voltage of 18 kW and a current of 20 mA with a scan speed of 0.5°/min and a 0.026° step size was employed to analyze the phase state and crystal structure of the synthesized NPs. The XRD patterns were obtained using a Smart Lab D/max 2500v/pc. The average grain sizes were calculated using the Debye–Scherrer formula. Specific surface area (SSA) of the synthesized NPs was determined using the BET method (Micromeritics Tristar 3000) by nitrogen adsorption at 77 K after degassing under flowing nitrogen at 150 °C for 3 h. X-ray photoelectron spectroscopy (XPS) conducted using a PHI1600 ESCA system was employed to characterize the chemical state of doped nitrogen and cerium atoms in the compounds as well as the other chemical ingredients of the synthesized samples. In the XPS process, an AlKa X-ray beam was used in a vacuum chamber at 2×10^{-10} Torr. The depth of analysis was 20–50 Å.

2.4. Photocatalytic activity measurement

An azo dye-MB aqueous solution with an initial concentration of 15 mg/L was employed as the model reactant to test the photocatalytic activity of the synthesized BT NPs and the $Ti_{1-x}Ce_xO_{1-y}N_y$ NPs. In order to detect the effects of various wavelength number for irradiation on the efficiency of MB photocatalytic degradation, a 30-W fluorescent lamp with a long-pass optical filter was used as the light source and five wavelengths (λ > 365 nm, λ > 420 nm, λ > 500 nm, λ > 550 nm and λ > 600 nm, respectively) were attained by using different long wavelength filters with intensity adjusted using a neutral density filter wheel. Then, 0.05 g of NPs was suspended in 50 ml of MB aqueous solution. The photocatalytic degradation of MB solute was followed by measuring its absorption in the range of 250–800 nm using a Varian Cary100 UV–vis spectrometer and the corresponding residue concentration of the MB solution was calculated using Lambert–Beer's law. The stability of as-prepared particles for the degradation of MB solution was evaluated with λ > 420 nm light using the same reaction system by running the reaction for five cycles. The concentration of photocatalyst in suspension was kept at 1 g/L. At the end of every cycle, the re-collected particles were washed several times using double distilled water till the residue solution was clear, and dried in a vacuum drier for 48 h at room temperature. All photocatalytic experiments were performed at room temperature. In order to demonstrate the reproducibility of our experiments, all photocatalytic reactions were repeated three times under identical conditions.

Table 1
Summary of SSA, XRD-determined average crystal size and BET-determined average size of synthesized (A) BT NPs and $Ti_{0.993}Ce_{0.007}O_{2-x}N_x$ (x = (B) 0.0000, (C) 0.0058, (D) 0.0070, (E) 0.0089) NPs.

	BT	CeT	CeNT-1	CeNT-2	CeNT-3
O% (at.%)	53.6	57.1	56.4	51.6	52.6
Ti% (at.%)	23.1	24.19	24.61	21.77	20.68
Ce (at.%)	0	0.71	0.69	0.70	0.72
x-Value					
N% (at.%)	0	0	0.52	0.70	0.89
y-Value					

3. Results and discussion

3.1. Chemical state analysis

The XPS of synthesized BT and $Ti_{1-x}Ce_xO_{1-y}N_y$ NPs is shown in Figs. 2–5, the detailed Ti 2p XPS in Fig. 2, the detailed O 1s XPS in Fig. 3, and the deconvoluted Ce 3d XPS, N 1s XPS in Figs. 4 and 5, with the elemental percentage shown in Table 1.

The chemical composition of the as-prepared samples is shown in Table 1, which illustrates that the composition of as-prepared NPs was Ti and O, with a trace amount of cerium and nitrogen dopant. In Table 1, we also determined the value of x to be 0.007, and the values of y to be 0.0000, 0.0058, 0.0070 and 0.0089, corresponding to 0.0 g, 1.0 g, 2.0 g and 3.0 g urea which were added into synthesis process, respectively. In order to simplify the names of samples, we denoted them as $Ti_{0.993}Ce_{0.007}O_{2-x}N_x$ (x = 0.0000, 0.0058, 0.0070 and 0.0089) throughout this paper.

Fig. 1 shows that Ti 2p binding energy increased from 458.2 eV for BT NPs to 458.5 eV for $Ti_{0.993}Ce_{0.007}O_{2-x}N_x$ (x = 0.0000) NPs and 458.7 eV for $Ti_{0.993}Ce_{0.007}O_{2-x}N_x$ (x = 0.0058, 0.0070 and 0.0089) NPs, respectively. This indicates that the Ti elements mainly existed as Ti^{4+}, and the fixation of doping Ce and N did not induce its chemical shift. The chemical shift of Ti 2p binding energy was not

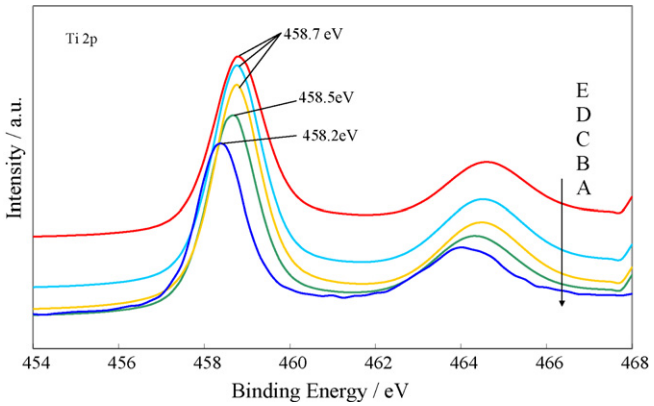

Fig. 1. (a) XRD patterns of (A) BT NPs and $Ti_{0.993}Ce_{0.007}O_{2-x}N_x$ (x = (B) 0.0000, (C) 0.0058, (D) 0.0070 and (E) 0.0089) NPs with varied amount of urea calcined at 550 °C for 2 h in air, and (b) high resolution in the range of 23–28° of (A) BT NPs and $Ti_{0.993}Ce_{0.007}O_{2-x}N_x$ (x = (B) 0.0000, (C) 0.0058, (D) 0.0070, (E) 0.0089) NPs with varied amount of urea calcined at 550 °C for 2 h in air.

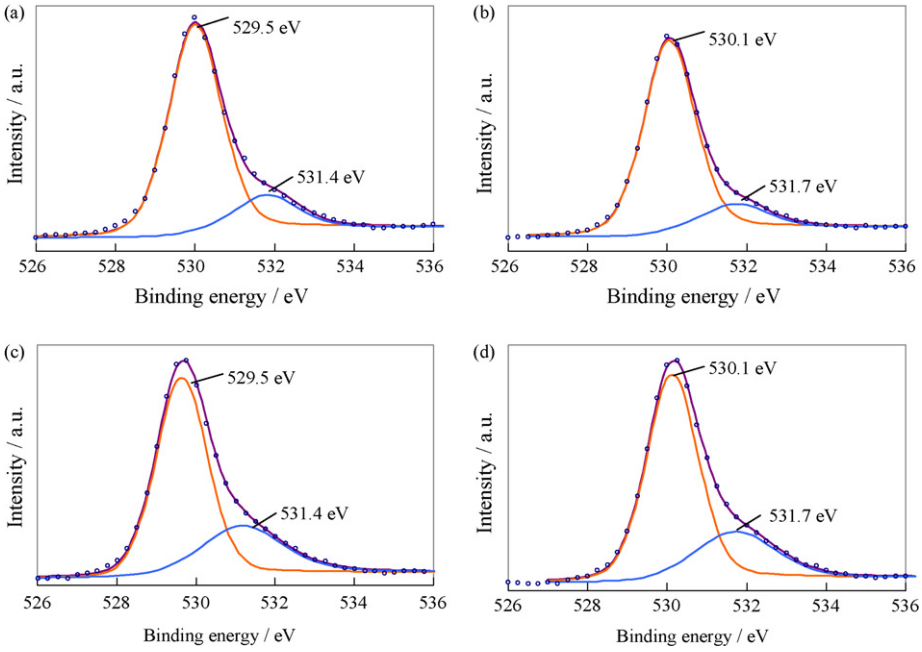

Fig. 2. Ti 2p XPS spectra with core level from 454 eV to 468 eV of synthesized (A) BT NPs and $Ti_{0.993}Ce_{0.007}O_{2-x}N_x$ (x = (B) 0.0000, (C) 0.0058, (D) 0.0070 and (E) 0.0089) NPs with varied amount of urea calcined at 550 °C for 2 h in air.

detected in any sample, which can be explained by the lack of reduction of the TiO_2 valence state as investigated by Gole et al. [19]. Compared to XPS of bare TiO_2 NPs, the 0.3 eV and 0.5 eV binding energy differences were found in $Ti_{0.993}Ce_{0.007}O_{2-x}N_x$ (x = 0.0000) NPs and $Ti_{0.993}Ce_{0.007}O_{2-x}N_x$ (x = 0.0058, 0.0070 and 0.0089) NPs, respectively. The lower binding energy resulted from the increased electron cloud density around Ti, which indicates that the atom possessing lower electronegativity was introduced into the TiO_2 crystal structure. It can also be further confirmed by the smaller electronegativity of N (3.04 Pauling electronegativity scale) than O (3.44 Pauling electronegativity scale).

In Fig. 2, the O 1s XPS spectrum shows a prominent peak at 530 eV, which was ascribed to the Ti–O bonds in TiO_2. From the deconvoluted spectrum, a peak at around 531.7 eV was detected. The oxygen species around this binding energy were first observed in native oxide. Then, it was identified as a Ti–O–N bond in titanium or titanium suboxides by Saha and Hadand [23]. Recently, the formation of oxynitride as investigated by Prokes et al. [29] has been accepted. Based on the reported results, it was assigned to the formation of oxynitride or Ti–O–Ce bond in this paper, because it became stronger with increasing amount of doping nitrogen.

Fig. 3 shows the Ce 3d XPS spectrum of $Ti_{0.993}Ce_{0.007}O_{2-x}N_x$ (x = 0.0000 and 0.0070) NPs. It was reported that Ce 3d spectra were assigned 3d 5/2 and 3d 3/2, two sets of spin orbital multiples [30,31]. From Fig. 4, we can see that the peak shape of Ce 3d XPS did not change after the incorporation of doping nitrogen. The existence of the +4 oxidation state was dominant in synthesized particles with a little +3 oxidation state giving rise to several peaks around 910–900 eV in $Ti_{0.993}Ce_{0.007}O_{2-x}N_x$ (x = 0.0000 and 0.0070) NPs, indicating the co-existence of Ce^{4+} and Ce^{3+} in $Ti_{0.993}Ce_{0.007}O_{2-x}N_x$ (x = 0.0000 and 0.0070) NPs. The binding energy of the Ce 2p5/2 peak at around 885.8 eV indicates the presence of CeO_2 species, and the peaks in the range of 910–900 eV were characterized by the presence of Ce_2O_3 [28,30–35]. Because the radii of Ce^{4+} (0.101 nm) and Ce^{3+} (0.111 nm) are both bigger than Ti^{4+} (0.068 nm), it is difficult to dope them into a TiO_2 crystal lattice and substitute Ti^{4+}. Therefore, it was deduced that a Ce–O–Ti bond formed at the interstitial sites or interfaces between CeO_2 and TiO_2. Increased numbers of generated hydroxyl groups can trap more photogenerated electrons due to an increased amount of Ce_2O_3 in $Ti_{0.993}Ce_{0.007}O_{2-x}N_x$ (x = 0.0070) NPs, which can be confirmed by the weaker electron configuration $(5d\ 6s)^0\ 4f^2\ O\ 2p^4$, $(5d\ 6s)^0\ 4f^1\ O\ 2p^5$ and $(5d\ 6s)^0\ 4f^0\ O\ 2p^6$ than $Ti_{0.993}Ce_{0.007}O_{2-x}N_x$ (x = 0.0000) NPs. Therein, electrons were trapped in Ce^{4+}/Ce^{3+} sites effectively. And subsequently, the recombination photogenerated electron–hole pairs were inhibited.

In Fig. 4, three core level peaks at 397.7 eV, 399.7 eV and 401.8 eV were detected in as-prepared $Ti_{0.993}Ce_{0.007}O_{2-x}N_x$ (x = 0.0058, 0.0070 and 0.0089) NPs from their deconvoluted N 1s XPS spectrum. We selected $Ti_{0.993}Ce_{0.007}O_{2-x}N_x$ (x = 0.0070) NPs to conduct the analysis here. It was clear that the element adjacent to nitrogen directly influences its binding energy and the stronger the electronegativity of the adjacent element, the higher the binding energy of nitrogen. In this paper, the first major peak at 397.7 eV was attributed to substitutional N species in the Ti–O–N structure, due to the fact that the binding energy was higher than that in N–Ti–N (397.3 eV), and the corresponding Ti 2p core level at 459.2 eV was significantly higher than that in TiN crystal (455.2 eV) [26]. When an oxygen atom was substituted for the nitrogen atom in a TiO_2

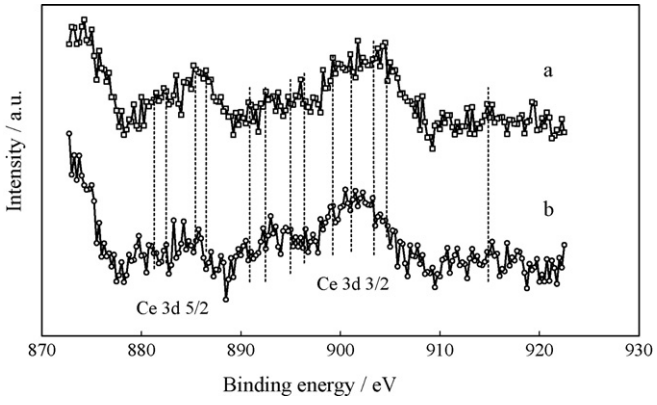

Fig. 3. O 1s XPS spectrum with the core level from 526 eV to 536 eV of synthesized $Ti_{0.993}Ce_{0.007}O_{2-x}N_x$ (x = (a) 0.0000, (b) 0.0058, (c) 0.0070 and (d) 0.0089) NPs with varied amount of urea calcined at 550 °C for 2 h in air.

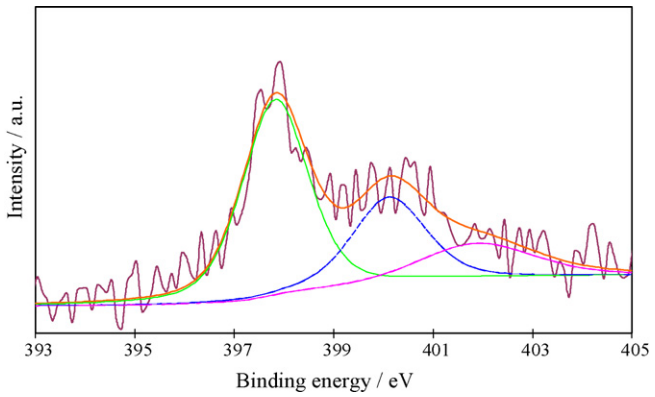

Fig. 4. Ce 3d deconvolution XPS spectrum with core level from 870 eV to 930 eV of synthesized $Ti_{0.993}Ce_{0.007}O_{2-x}N_x$ (x = (a) 0.0000 and (b) 0.0070) NPs with varied amount of urea calcined at 550 °C for 2 h in air.

lattice, the electron density around N 1s could have been reduced while that around Ti 2p increased, which then induced an increase in N binding energy and a decrease in Ti 2p binding energy in prepared NPs. The second peak at 399.5 eV was attributed to the adsorbed NO or N species in Ti–N–O linkage [23]. The third peak at 401.8 eV was attributed to molecularly adsorbed N species on the surface of the nitrogen modified titanium dioxide NPs [3,4], or the formation of interstitial Ti–N bonding [26]. The latter was unlikely in this present work because the nitrogen atoms in interstitial sites existed in a higher oxidized state. For this reason, we assigned the peak at 401.8 eV to molecularly adsorbed N species on the surface of the particles. These nitrogen species can be desorbed at a low temperature [22], or annealed away by heating the particles at temperature in excess of 550 °C in vacuum [24]. It was likely that the chemisorbed nitrogen did not contribute to catalytic activity.

3.2. Crystal structure analysis

XRD patterns of synthesized BT and $Ti_{0.993}Ce_{0.007}O_{2-x}N_x$ (x = 0.0000, 0.0058, 0.0070 and 0.0089) NPs were shown in Fig. 5a and b. A summary of SSA, crystalline structure and XRD-determined average crystal size is shown in Table 2. Fig. 5a indicates that the crystallinity was suppressed by the amount of doping with cerium and nitrogen, and this trend was strengthened with the doping amount increasing. Meanwhile, the growth of crystal size of NPs was suppressed to different extent by the doping impurities, which can be ascribed to the segregation of the doping ions at the grain boundary, in turn due to the bigger ionic radii of Ce^{3+} (0.111 nm) and Ce^{4+} (0.101 nm) than Ti^{4+} (0.068 nm), where it was difficult for Ce^{3+} and Ce^{4+} to replace Ti^{4+} in the crystalline lattice. No peaks other than anatase were detected in Fig. 1a, which confirmed that all doping cerium and nitrogen had been incorporated into a TiO_2 crystal structure. From Fig. 5b, we can see that the width of anatase 1 0 1 crystal plane peak broadened as the nitrogen doping amount was increased. At the same time, the grain

Table 2
Elemental percentages determined by XPS of synthesized $Ti_{1-x}Ce_xO_{1-y}N_y$ NPs.

Synthesized NPs	XRD analysis		BET analysis
	Crystal size[a] d (nm)	Space (Å)	SSA (m^2/g)
A	11.12	3.50	71.24
B	10.60	3.51	90.79
C	9.89	3.51	85.32
D	9.76	3.51	83.42
E	9.75	3.52	88.01

[a] Calculated from anatase 1 0 1 crystal face.

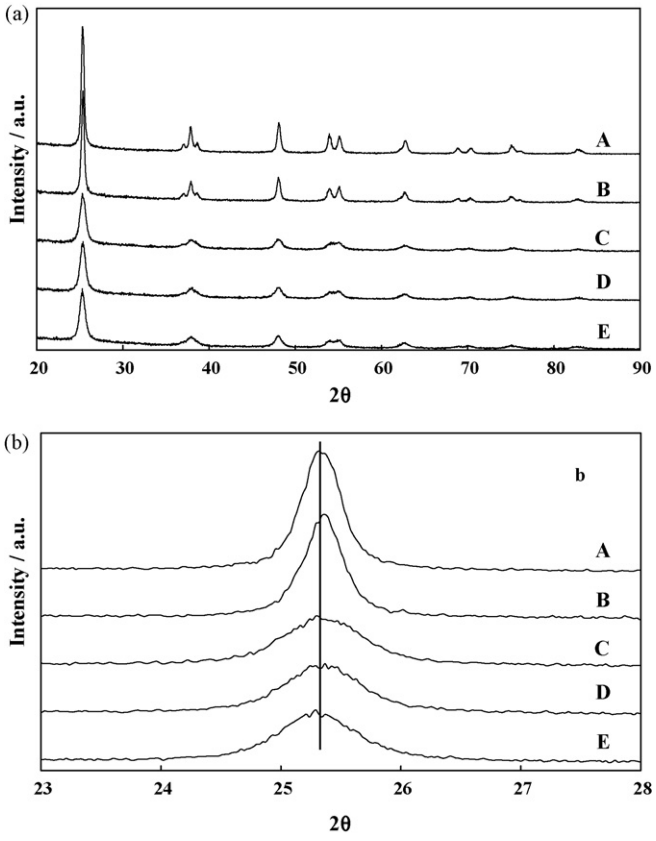

Fig. 5. N 1s deconvolution XPS spectrum with core level from 397 eV to 402 eV of synthesized $Ti_{0.993}Ce_{0.007}O_{2-x}N_x$ (x = 0.0070).

sizes of $Ti_{0.993}Ce_{0.007}O_{2-x}N_x$ (x = 0.0058, 0.0070 and 0.0089) NPs were all smaller than $Ti_{0.993}Ce_{0.007}O_{2-x}N_x$ (x = 0.0000) NPs, which is consistent with the results calculated by Scherrer's formula. It has been thought that doping nitrogen reduced the crystallization of anatase and retarded the transformation of amorphous titanium dioxide to anatase, possibly due to the decomposition of surplus urea in the mixture that might restrain the formation and growth of the TiO_2 crystal phase during the solid reaction process [13]. In Table 2, no distinct change of d space (d = 0.35 nm) was observed in all experimental NPs, which demonstrates that anatase crystal structure was still the predominant crystal phase. All as-synthesized NPs with non-porous surface were confirmed by adsorption–desorption isotherm (which is not shown here). In Table 2, a larger SSA of $Ti_{0.993}Ce_{0.007}O_{2-x}N_x$ (x = 0.0058, 0.0070 and 0.0089) NPs was observed than the BT and $Ti_{0.993}Ce_{0.007}O_{2-x}N_x$ (x = 0.0000) NPs, which can be attributed to the decreased particle size resulting from the doping process.

3.3. Photocatalytic activities and mechanism analysis

The efficiency of photocatalytic degradation of MB aqueous solution with various prepared NPs under visible light (λ > 420 nm) is shown in Fig. 6. In order to evaluate the photocatalytic activities of single doped particles and double doped particles, the nitrogen-doped TiO_2 (denoted as NT) NPs were also prepared here using the same method as described in Section 2.2. The enhanced photocatalytic activity of $Ti_{0.993}Ce_{0.007}O_{2-x}N_x$ (x = 0.0070) NPs was attributed to the co-effect of doping with nitrogen and cerium in as-prepared NPs. Doping with Ce ions served as the electron trap in the reaction because of their varied valences and special 4f level [32,26,15]. Meanwhile, doping with nitrogen narrowed the band gap of $Ti_{0.993}Ce_{0.007}O_{2-x}N_x$ (x = 0.0058, 0.0070 and

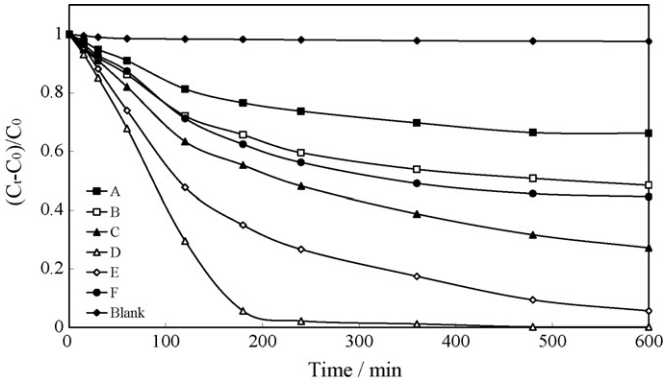

Fig. 6. Efficiency of photocatalytic degradation of MB aqueous solution in the presence of prepared (A) BT NPs, $Ti_{0.993}Ce_{0.007}O_{2-x}N_x$ (x = (B) 0.0000, (C) 0.0058, (D) 0.0070, (E) 0.0089) NPs and (F) NT NPs under visible light ($\lambda > 420$ nm).

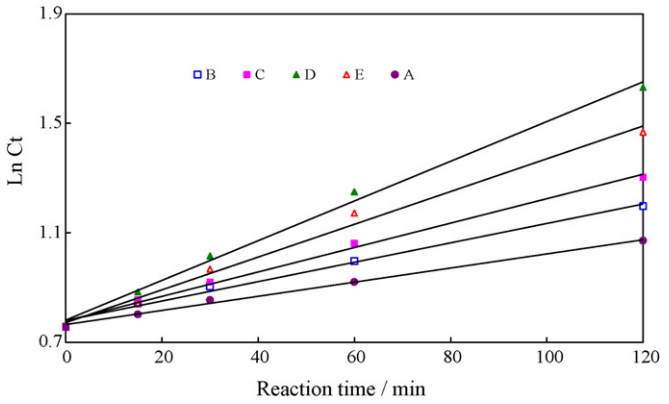

Fig. 7. Plots of photocatalytic degradation of MB variations in $\ln(C_t)$ as a function of irradiation time and linear fits of (A) BT NPs and $Ti_{0.993}Ce_{0.007}O_{2-x}N_x$ (x = (B) 0.0000, (C) 0.0058, (D) 0.0070 and (E) 0.0089) NPs.

0.0089) NPs to enhance their absorption within the visible light region. The decreased photocatalytic activities were found with too many doping impurities, such as $Ti_{0.993}Ce_{0.007}O_{2-x}N_x$ ($x = 0.0089$) NPs, which can be explained by saying that overfull dopants can act as recombination centers. In Fig. 6, synthesized cerium and nitrogen co-doped TiO_2 NPs (except for $Ti_{0.993}Ce_{0.007}O_{2-x}N_x$ ($x = 0.0058$) NPs) exhibited a higher photocatalytic activity than BT and $Ti_{0.993}Ce_{0.007}O_{2-x}N_x$ ($x = 0.0000$) NPs. It has been confirmed by Turchi and Ollis [36] that the •OH radicals are the primary source of oxidation in a photocatalytic system. When cerium was incorporated into a TiO_2 crystal structure, a large numbers of •OH radicals were generated due to the co-existence of Ce^{4+}/Ce^{3+} ion pairs, as illustrated by the following equations [28]:

$$Ce^{4+} + e^- \rightarrow Ce^{3+} \quad (1)$$

$$Ce^{3+} + O_2 \rightarrow O_2^{\bullet -} + Ce^{4+} \quad (2)$$

$$h^+ + H_2O \rightarrow {}^\bullet OH + H^+ \quad (3)$$

$$O_2^{\bullet -} + 2H^+ \rightarrow 2{}^\bullet OH \quad (4)$$

These photogenerated •OH radicals had a positive effect on the basis of organic reactant. It should be pointed out that bare TiO_2 photocatalyst exhibits a significant removal of MB under visible light (>420 nm) irradiation, which can be ascribed to adsorption of reactant and slight dye self-sensitization. Moreover, it was reported that MB can absorb visible light and photocatalytically degrade itself to some extent. Therefore, the actual degradation efficiency was calculated considering these factors and the MB solution without any photocatalyst being irradiated under fluorescent light and visible light (>420 nm) for 6 h for comparison in this paper.

3.4. Kinetics of photocatalytic process analysis

Fig. 7 shows photocatalytic degradation of MB variations in $\ln(C_t)$ as a function of irradiation time and linear fitting curves of $Ti_{0.993}Ce_{0.007}O_{2-x}N_x$ NPs. The summary of the first-order kinetics of as-prepared NPs under visible light ($\lambda > 420$ nm) within the initial 2 h is shown in Table 3.

From the experimental results showed in Fig. 6, it is plausible to suggest that the reactions followed the first-order kinetics according to the Langmuir–Hinshelwood (LH) model within the initial 2 h. The LH kinetic equation was mostly used to explain the kinetics of the heterogeneous catalytic processes as given by:

$$r = -\frac{dC}{dt} = \frac{k_r KC}{1 + KC} \quad (5)$$

where r represents the rate of reaction that changes with time (t). The rate expression based on LH expression can be reduced to first-order kinetics when $t = 0$, $C = C_0$, it was described as follows:

$$-\ln\left(\frac{C}{C_0}\right) = k_r t \quad (6)$$

where k_r represents the apparent rate constant, C represents the MB concentration in aqueous solution at any time t during photocatalytic degradation, and t is reaction time. It was demonstrated that the current photocatalytic degradation process was in good accordance with first-order kinetics resulting from the linear correlation between $\ln(C_t)$ and t. The apparent rate constant k was found in the order of $Ti_{0.993}Ce_{0.007}O_{1.993}N_{0.007}$ > $Ti_{0.993}Ce_{0.007}O_{1.9911}N_{0.0089}$ > $Ti_{0.993}Ce_{0.007}O_{1.9942}N_{0.0058}$ > $Ti_{0.993}Ce_{0.007}O_{2.000}N_{0.000}$ > BT under visible light (>420 nm). It should be pointed out that the first-order apparent rate constant was not proportional to the amount of doping cerium and nitrogen after it reached 0.7 at.% Ce and 0.7 at.% N, which means that the optimal doping percentage was found within the studied range, which is consistent with the results shown in Fig. 6.

3.5. Effects of photocatalytic parameters analysis

Two experimental parameters were selected to investigate their effects on MB photocatalytic degradation: the atomic ratio of doped N to Ce and the irradiation wavelength number.

Fig. 8 shows the efficiency of photocatalytic degradation of MB under various wavelengths of light ($\lambda > 365$ nm, $\lambda > 420$ nm, $\lambda > 500$ nm, $\lambda > 550$ nm and $\lambda > 600$ nm) in the presence of suspended $Ti_{0.993}Ce_{0.007}O_{2-x}N_x$ NPs for 6 h. It is well known that the capacity of photogenerated electrons during the photocatalytic process mainly depends on the intensity of the incident photons with matchable energy for irradiation. It was necessary to the impact of wavelength number for irradiation on photocatalytic efficiency. Fig. 6 shows results of photocatalytic degradation of MB versus various wavelength numbers for irradiation in the presence of $Ti_{0.993}Ce_{0.007}O_{2-x}N_x$ NPs suspension for 6 h. Here, $Ti_{0.993}Ce_{0.007}O_{1.993}N_{0.007}$ NPs were selected as model photocat-

Table 3
Summary of the pseudo-first-order kinetics of various prepared NPs under visible light ($\lambda > 420$ nm) within the initial 2 h.

Sample ID	Fitted equation	R^2	Rate constant
BTNPs	$y = 0.0026x + 0.7645$	0.9961	0.0026
$Ti_{0.993}Ce_{0.007}O_{2.000}N_{0.0000}$ NPs	$y = 0.0045x + 0.7781$	0.9945	0.0045
$Ti_{0.993}Ce_{0.007}O_{1.9942}N_{0.0058}$ NPs	$y = 0.0035x + 0.7797$	0.9908	0.0035
$Ti_{0.993}Ce_{0.007}O_{1.993}N_{0.0070}$ NPs	$y = 0.0073x + 0.7806$	0.9948	0.0073
$Ti_{0.993}Ce_{0.007}O_{1.9911}N_{0.0089}$ NPs	$y = 0.006x + 0.7715$	0.9905	0.0060

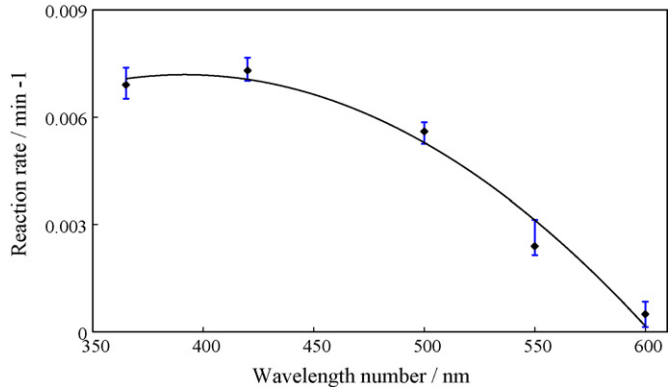

Fig. 8. Plots of efficiency of photocatalytic degradation of MB versus various wavelength numbers for irradiation in the presence of $Ti_{0.993}Ce_{0.007}O_{2-x}N_x$ NPs suspension for 6 h. Each point represents an average value of three or more separate experiments and the vertical line represents the error associated with each reading expressed as standard deviation.

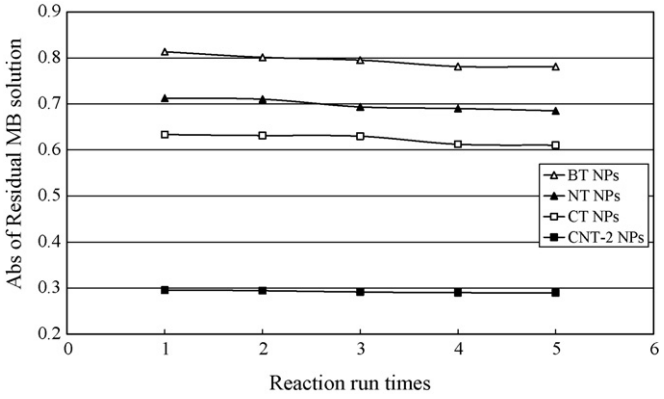

Fig. 10. Stabilities of as-prepared particles for the photocatalytic degradation of MB aqueous solution under visible light (λ > 420 nm) irradiation.

alysts to carry out the following experiments due to their high efficiency. As observed in Fig. 8, a slightly decreased efficiency was observed under λ > 365 nm light compared to the experimental results under λ > 420 nm light irradiation, which indicated that the TiO_2 NPs co-doping cerium and nitrogen acted as a visible response semiconductor and the co-doped cerium and nitrogen acted as a recombination center for the photogenerated carriers in the UV light spectrum. At wavelength numbers λ > 500 nm, $Ti_{0.993}Ce_{0.007}O_{1.993}N_{0.007}$ NPs still displayed notable activity relative to the experimental results under λ > 420 nm light irradiation but differences in activity were muted at wavelengths λ > 550 nm and λ > 600 nm, which resulted from the various extents of band gap narrowed by the doping impurities.

Fig. 9 shows the relationship between the atomic ratio of doping N to Ce and the efficiency of photocatalytic degradation of MB under visible light (>420 nm). In order to investigate the effects of the atomic ratio of doping N to Ce on the efficiency of photocatalytic degradation of MB, $Ti_{0.993}Ce_{0.007}O_{2-x}N_x$ ($x = 0.0040$ and 0.0110) NPs were also prepared using the same method described in Section 2.2. The experimental results in Fig. 7 clearly demonstrated that the apparent rate strongly related to the atomic ratio of doping N to Ce. It was accepted that the photoreaction was initiated by the photogenerated electron and hole pairs and the generation/separation of photogenerated e^-–h^+ pairs, and the transformation of photons to carriers, i.e., quantum efficiency, are all key factors in the photocatalytic process [37]. The initial reaction rate increased with increased the dopants cerium and nitrogen amounts increasing first. And then the degradation rate showed a maximum when the dopant amount reached 0.7 at.% Ce and 0.7 at.% N. With further increases in the dopant amounts, the decomposition rate decreased, which can be ascribed to the formation of a recombination center of photogenerated e^-–h^+ pairs. It was explained for synthesized NPs, the 4f level plays an important role in interfacial charge transfer, and cerium ions can act as an effective electron scavenger. Moreover, the existence of Ce^{4+}/Ce^{3+} pairs created a charge imbalance, resulting in more hydroxide ions adsorbed on the surface. The adsorbed hydroxide ions act as traps that inhibit recombination of photogenerated e^-–h^+ pairs as well. It should be pointed out that no distinct changes in SSA or particle size were observed (Table 2) among these as-synthesized particles, so the recombination of photogenerated e^-–h^+ was assigned to the key factor for the decreased efficiency of photocatalytic degradation of MB. So, the interfacial charge transfer being a determining-rate step for photocatalytic reaction was determined in this paper.

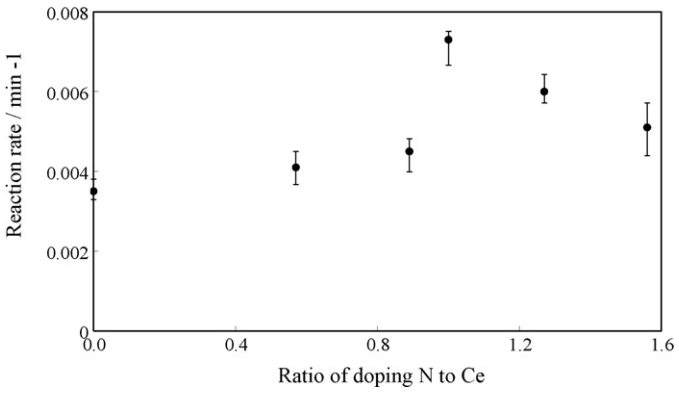

Fig. 9. Relationship between the atomic ratio of doping N to Ce in prepared $Ti_{0.993}Ce_{0.007}O_{2-x}N_x$ and the efficiency of photocatalytic degradation of MB under visible light (>420 nm) irradiation. Each point represents an average value of three or more separate experiments and the vertical line represents the error associated with each reading expressed as standard deviation.

3.6. Stability of photocatalyst

Fig. 10 shows the stability of the as-prepared photocatalyst for MB solution degradation. Based on the results reported in Fig. 6, we selected BT NPs, NT NPs, CT NPs and $Ti_{0.993}Ce_{0.007}O_{1.993}N_{0.007}$ NPs as model photocatalysts to carry out the stability evaluation experiments. In addition, from Fig. 6, we can see that for $Ti_{0.993}Ce_{0.007}O_{1.993}N_{0.007}$ NPs, when the reaction was run over 3 h, the MB can be decomposed completely, so we selected the initial 2 h as the reaction duration in the stability evaluation experiments. It is evident from Fig. 10 that $Ti_{0.993}Ce_{0.007}O_{1.993}N_{0.007}$ NPs are more stable that BT NPs, NT NPs and CT NPs, while the similar stabilities were found for the NT NPs and CT NPs. Overall, the results here show a clear relationship between the types of synthesized NPs and stability.

4. Conclusions

Cerium and nitrogen co-doped anatase TiO_2 NPs were successfully synthesized using a one-step technique with a modified sol–gel process. The best experimental result for the photocatalytic degradation of a MB aqueous solution under visible light (λ > 420 nm) was found with $Ti_{0.993}Ce_{0.007}O_{2-x}N_x$ ($x = 0.0070$) NPs, which was confirmed by the reaction rate constant of first-order kinetics calculated using the LH model. The interfacial charge transfer was determined to be a key step for photocatalytic reaction in the current study. The synergistic effect of doping with cerium

and nitrogen together effectively inhibited the recombination of photogenerated electrons and holes.

Acknowledgement

This project was financial supported by National Natural Science Foundation of China (20776103).

References

[1] A. Fujishima, K. Honda, Electrochemical photolysis of water at a semiconductor electrode, Nature 238 (1972) 37–38.
[2] B. O'Regan, M. Gratzel, A low cost high-efficiency solar cell based on dye-sensitized colloidal TiO_2 films, Nature (London) 353 (1991) 737–739.
[3] S. Sato, Photocatalytic activity of NO_x-doped TiO_2 in the visible light region, Chem. Phys. Lett. 123 (1986) 126–128.
[4] R. Asahi, T. Ohwaki, K. Aoki, Y. Taga, Visible-light photocatalysis in nitrogen-doped titanium oxides, Science 293 (2001) 269–271.
[5] A. Fujishima, T.N. Rao, D.A. Tryk, Titanium dioxide photocatalysis, J. Photochem. Photobiol. C: Photochem. Rev. 1 (2000) 1–21.
[6] J.J. Xu, Y.H. Ao, D.G. Fu, Study on photocatalytic performance and degradation kinetics of X-3B with lanthanide-modified titanium dioxide under solar and UV illumination, J. Hazard. Mater. 164 (2009) 762–768.
[7] Z.G. Zou, J.H. Ye, H. Arakawa, Photocatalytic water splitting into H_2 and/or O_2 under UV and visible light irradiation with a semiconductor photocatalyst, Int. J. Hydrogen Energy 28 (2003) 663–669.
[8] M.R. Hoffmann, S.T. Martin, W. Choi, D.W. Bahnemannt, Environmental applications of semiconductor photocatalysis, Chem. Rev. 95 (1995) 69–96.
[9] M.A. Fox, M.T. Dulay, Heterogeneous photocatalysis, Chem. Rev. 93 (1993) 341.
[10] F.B. Li, X.Z. Li, M.F. Hou, K.W. Cheah, W.C.H. Choy, Enhanced photocatalytic activity of Ce^{3+}–TiO_2 for 2-mercaptobenzothiazole degradation in aqueous suspension for odour control, Appl. Catal. A: Gen. 285 (2005) 181–189.
[11] N. Sasirekha, S. John, S. Basha, K. Shanthi, Photocatalytic performance of Ru doped anatase mounted on silica for reduction of carbon dioxide, Appl. Catal. B: Environ. 62 (2006) 169–180.
[12] K. Nagaveni, M.S. Hegde, G. Madras, Structure and photocatalytic activity of $Ti_{1-x}M_xO_{2\pm\delta}$ (M = W, V, Ce, Zr, Fe, and Cu) synthesized by solution combustion method, J. Phys. Chem. B 108 (2004) 20204–20212.
[13] W.K. Jo, J.T. Kim, Application of visible-light photocatalysis with nitrogen-doped or unmodified titanium dioxide for control of indoor-level volatile organic compounds, J. Hazard. Mater. 164 (2009) 360–366.
[14] M.I. Litter, J.A. Navio, Photocatalytic properties of iron-doped titania semiconductors, J. Photochem. Photobiol. A: Chem. 98 (1996) 171–181.
[15] J.C.S. Wu, C.H. Chen, A visible-light response vanadium-doped titania nanocatalyst by sol–gel method, J. Photochem. Photobiol. A: Chem. 163 (2004) 509–515.
[16] P. Zabek, J. Eberl, H. Kisch, On the origin of visible light activity in carbon-modified titania, Photochem. Photobiol. Sci. 8 (2009) 264–269.
[17] W.Z. Yang, C. Chen, F.Q. Wu, Photodegradation of rhodamine B under visible light by bimetal codoped TiO_2 nanocrystals, J. Hazard. Mater. 164 (2009) 615–620.
[18] Y. Izumi, T. Itoi, S. Peng, Structure and photocatalytic role of sulfur or nitrogen-doped titanium oxide with uniform mesopores under visible light, J. Phys. Chem. C 113 (2009) 6706–6718.
[19] J.L. Gole, D. John, C. Burda, Y.B. Lou, X.B. Chen, Highly efficient formation of visible light tunable $TiO_{2-x}N_x$ photocatalysts and their transformation at the nanoscale, J. Phys. Chem. B 108 (2004) 1230–1240.
[20] S. Sakthivel, M. Janczarek, H. Kisch, Visible light activity and photoelectrochemical properties of nitrogen-doped TiO_2, J. Phys. Chem. B 108 (2004) 19384–19387.
[21] H. Irie, Y. Watanabe, K. Hashimoto, Nitrogen-concentration dependence on photocatalytic activity of $TiO_{2-x}N_x$ powders, J. Phys. Chem. B 107 (2003) 5483–5486.
[22] O. Diwald, T.L. Thompson, T. Zubkov, E.G. Goralski, S.D. Walck, J.T. Yates Jr., Photochemical activity of nitrogen-doped rutile TiO_2 (1 1 0) in visible light, J. Phys. Chem. B 108 (2004) 6004–6008.
[23] C.N. Saha, G.T. Hadand, Titanium nitride oxidation chemistry: an X-ray photoelectron spectroscopy study, J. Appl. Phys. 72 (1992) 3072–3079.
[24] E. Gyorgy, A.P. Pino, P. Serra, J.L. Morenza, Depth profiling characterisation of the surface layer obtained by pulsed Nd:YAG laser irradiation of titanium in nitrogen, Surf. Coat. Technol. 173 (2003) 265–270.
[25] D. Li, H. Haneda, S. Hishata, N. Ohashi, Synthesis by spray pyrolysis and surface characterization, Chem. Mater. 17 (2005) 2588–2595.
[26] H. Wei, W. Wu, N. Lun, F. Zhao, Preparation and photocatalysis of TiO_2 Nanoparticles co-doped with nitrogen and lanthanum, J. Mater. Sci. 4 (2004) 1305–1308.
[27] Y. Sakatani, J. Nunoshige, H. Ando, K. Okusako, H. Koike, T. Takata, J.N. Kondo, M. Hara, K. Domen, Photocatalytic decomposition of acetaldehyde under visible light irradiation over La^{3+} and N Co-doped TiO_2, Chem. Lett. 32 (2003) 1156–1157.
[28] C. Liu, X.H. Tang, C.H. Mo, Z.M. Qiang, Characterization and activity of visible-light-driven TiO_2 photocatalystcodoped with nitrogen and cerium, J. Solid State Chem. 181 (2008) 913–919.
[29] S.M. Prokes, J.L. Gole, X.B. Chen, Defect-related optical behavior in surface-modified TiO_2 nanostructures, Adv. Funct. Mater. 15 (2005) 161–167.
[30] M.R. Benjaram, A. Khan, Y. Yamada, T. Kobayashi, S. Loridant, Structural characterization of CeO_2–TiO_2 and V_2O_5/CeO_2–TiO_2 Catalysts by Raman and XPS techniques, J. Phys. Chem. B 107 (2008) 5162–5167.
[31] Z.L. Liu, B. Guo, L. Hong, H. Jiang, Preparation and characterization of cerium oxide doped TiO_2 nanoparticles, J. Phys. Chem. Solid 66 (2005) 161–167.
[32] W. Xu, Y. Gao, H.Q. Liu, The Preparation, Characterization, and their photocatalytic activities of rare-earth-doped TiO_2 nanoparticles, J. Catal. 207 (2002) 151–157.
[33] K.T. Ranjit, I. Willner, S.H. Bossmann, A.M. Braun, Lanthanide oxide doped titanium dioxide photocatalysts: effective photocatalysts for the enhanced degradation of salicylic acid and *t*-cinnamic acid, J. Catal. 204 (2001) 305–313.
[34] K.T. Ranjit, I. Willner, S.H. Bossmann, A.M. Braun, Lanthanide oxide-doped titanium dioxide photocatalysts: novel photocatalysts for the enhanced degradation of *p*-chlorophenoxyacetic acid, Environ. Sci. Technol. 35 (2001) 1544–1549.
[35] B.M. Reddy, A. Khan, Y. Yamada, T. Kobayashi, S. Loridant, J. Volta, Raman and X-ray photoelectron spectroscopy study of CeO_2–ZrO_2 and V_2O_5/CeO_2–ZrO_2 catalysts, Langmuir 19 (2003) 3025–3030.
[36] C.S. Turchi, D.F. Ollis, Photocatalytic degradation of organic water contaminants: mechanism involving hydroxyl radical attack, J. Catal. 122 (1990) 178–192.
[37] X.G. Hou, F.H. Hao, B. Fan, X.N. Gu, X.Y. Wu, A.D. Liu, Modification of TiO_2 photocatalytic films by V+ ion implantation, Nucl. Instrum. Method Phys. Res. B 243 (2006) 99–102.